SAR Imaging from Partial-Aperture Data with Frequency-Band Omissions

Müjdat Çetin[a] and Randolph L. Moses[b]

[a]Laboratory for Information and Decision Systems, Massachusetts Institute of Technology, 77 Massachusetts Ave., Cambridge, MA 02139, USA

[b]The Ohio State University, Department of Electrical and Computer Engineering 2015 Neil Avenue, Columbus, OH 43210, USA

ABSTRACT

We consider the problem of wide-angle SAR imaging from data with arbitrary frequency-band omissions. We propose an approach that involves composite image formation through combination of subaperture images, as well as point-enhanced, superresolution image reconstruction. This framework provides a number of desirable features including preservation of anisotropic scatterers that do not persist over the full wide-angle aperture; robustness to bandwidth limitations and frequency-band omissions; as well as a characterization of the aspect dependence of scatterers. We present experimental results based on the Air Force Research Laboratory (AFRL) "Backhoe Data Dome," demonstrating the effectiveness of the proposed approach.

Keywords: synthetic aperture radar, wide-angle imaging, sparse-aperture imaging, feature-enhanced imaging, inverse problems, superresolution

1. INTRODUCTION

Traditional image formation techniques for synthetic aperture radar (SAR) rely on data on a *narrow-angle*, *filled* aperture. In particular, it is customary to assume that the phase history data lie in an (almost rectangular) annular region in the 2-D spatial frequency domain, establishing a filled synthetic aperture in both the angle (azimuth) and the frequency (range) direction. This is based on the fact that many traditional systems integrate over relatively small angles (typically on the order of a few degrees) and transmit over an uninterrupted portion of the frequency spectrum. However, there are a number of emerging applications where neither of these assumptions holds. One such application is monostatic wide-angle imaging, which may be used to obtain ultra-high resolution at relatively high operating frequencies, or to compensate for the reduced resolution in relatively low frequencies. The data in wide-angle sensing usually lie in a narrow arc in the spatial frequency domain, which constitutes a sparse aperture since the data support fills only a small portion of the circumscribing rectangle. A number of recent technology advancements enable consideration of wide-angle imaging. First, advancements in GPS and INS systems permit collection of coherent data across longer times and flight paths. Second, unmanned air vehicle (UAV) technology and collaboration among UAVs provide a number of wide-angle imaging possibilities. UAVs can, in many applications, fly closer to the scene of interest, and thus can traverse a wider-angle aperture in a given amount of time compared to a platform with a greater standoff distance. A second application of interest is foliage penetration (FOPEN) radar, which operates at the VHF/UHF bands. At these relatively low frequencies, it is likely that we will not be able to use an uninterrupted frequency band, due to the existence of other in-band radiators and FCC licenses. As a result, the data will contain frequency-band omissions resulting in a non-traditional, sparse (or at least not filled) aperture. More broadly, partial aperture data involving omissions in the frequency band may be encountered in higher frequencies as well, due to a number of reasons including jamming and data dropouts. A third application involves bistatic and multistatic imaging. One scenario is a bistatic/multistatic radar operation, in which a distant standoff platform acts as the transmitter and one or more

Further author information:
Müjdat Çetin: E-mail: mcetin@mit.edu
Randolph L. Moses: E-mail: moses.2@osu.edu

UAVs act as (closer-in) receivers. UAVs working in tandem can collect angular subapertures which can then be combined into a wider aperture which potentially involves omissions in the frequency and/or angle bands.

When traditional image formation techniques are applied to wide-angle data with frequency-band omissions, they often yield unsatisfactory results, making the resulting images difficult to interpret and of limited value for further processing. This is due to a number of reasons. First, the point spread function (PSF) of an isotropic point scatterer coherently imaged over a wide-angle aperture is more irregular than the more customary sinc-like PSFs encountered in traditional SAR imaging, leading to sidelobes that might interfere with other scatterers in the scene. Second, when there are frequency-band omissions, the PSFs resulting from conventional imaging become even more irregular, causing yet more pronounced artifacts in the reconstructed images. Furthermore, different types of band omissions lead to different kinds of artifacts, making it a very challenging task to adapt to and interpret the formed imagery. Third, in a wide-angle imaging scenario, the isotropic point scattering assumption employed by conventional imaging does not usually hold, as many scatterers do not persist over such wide apertures and exhibit some aspect dependence. In such a scenario, conventional imaging can lead to inaccuracies in relative reflectivities of scatterers with different levels of anisotropy. Furthermore, such processing only produces a reflectivity estimate of each scatterer but does not characterize its aspect dependence. Yet, such aspect dependence (if accurately extracted) can itself be an important feature for scene interpretation, e.g. for target recognition.

Motivated by these observations, we explore new image formation strategies for wide-angle data with frequency-band omissions. In particular, we consider the combination of two ideas based on our previous work: composite wide-angle image formation based on subaperture images,[1] and model-based, point-enhanced superresolution imaging.[2] Composite image formation aims to address the issue of limited scattering persistence in wide-angle imaging. The idea is to form subaperture images from narrower-angle subsets of the data, and then form a composite image through a nonlinear combination of these subaperture images. When conventional Fourier transform-based imaging is used to form the subaperture images, composite imaging still suffers from artifacts due to the irregular PSFs, especially in cases involving low-bandwidth data or frequency-band omissions. To address these issues, we propose using point-enhanced imaging[2] to form the subaperture images. This technique uses an explicit model of the observation process (hence incorporates information about the structure of the partial aperture), and as a result, is more robust to data limitations. Furthermore this framework also allows the incorporation of prior information about the underlying scene, which can lead to superresolution. Given such point-enhanced subaperture images, we again form a composite image. This imaging strategy produces not only a reflectivity estimate for each spatial location, but also some information on aspect dependence. We present experimental results based on the Air Force Research Laboratory (AFRL) "Backhoe Data Dome,"[3] demonstrating the effectiveness of the proposed approach.

2. WIDE-ANGLE IMAGING WITH FREQUENCY-BAND OMISSIONS

Let us consider a wide-angle imaging scenario with a center frequency of 10 GHz, an angular aperture of 110°, and a bandwidth of 500 MHz. Fig. 1 shows the magnitude image and the frequency support of the simulated Hamming-windowed data from an isotropic point scatterer in such a scenario. We now use this example to discuss image formation strategies from such data as well as partial aperture data with frequency-band omissions.

2.1. Coherent Integration with an Isotropic Scattering Assumption

The conventional processing we consider here interpolates the phase history data lying on a narrow arc to a Cartesian grid, performs zero-padding to fill the circumscribing rectangle (see Fig. 1), and then takes an inverse 2-D Fourier transform to reconstruct the image. Such processing of the data shown in Fig. 1 leads to the PSF in Fig. 2(a). The curved data support leads to this shape of the PSF which is quite different from the sinc-like PSFs of traditional narrow-angle SAR. This PSF is indicative of the types of artifacts that are likely to appear in conventional images of isotropic scatterers from wide-angle data. Here we have assumed that we have the entire 500 MHz band of data. Now let us consider the case where we have omissions in the frequency band. In particular, let us consider the two masks in Fig. 3, indicating two patterns of band omissions leading to 70% and 30% of the data being available, respectively. In Fig. 2(b) and 2(c) we show the PSFs that result from conventional imaging in the case of such partial aperture data with frequency-band omissions. These PSFs

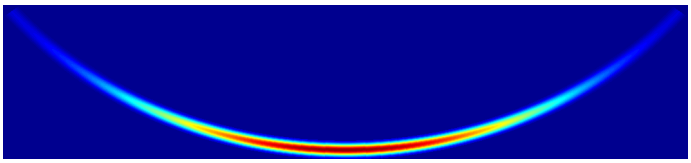

Figure 1. Magnitude image and frequency support of Hamming-windowed data from an isotropic point scatterer over a 110° aperture. Center frequency is 10 GHz and bandwidth is 500 MHz.

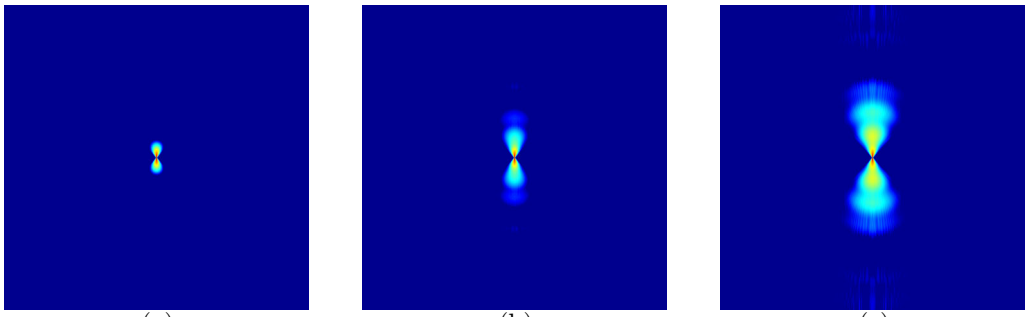

(a) (b) (c)

Figure 2. Conventional images of a point scatterer based on the data shown in Fig. 1. The images show a region of 10×10 meters. Vertical and horizontal directions in the images correspond to range and cross-range respectively. The images are in logarithmic scale and show the top 40dB of the responses. (a) Full frequency band available. (b) 70% of the frequency band available (based on the mask in Fig. 3(a)). (c) 30% of the frequency band available (based on the mask in Fig. 3(b)).

exhibit significant, wide lobes, suggesting that conventional imaging will cause severe artifacts in these scenarios. In these illustrative examples, we have considered an isotropic point scatterer. Of course, another problem with conventional imaging is that most scatterers will not persist over such wide-angle apertures, and the isotropic scattering assumption will fail. This is an issue we address in the next section.

2.2. Composite Image Formation

In order to accommodate the aspect dependence of the scatterers, we have considered a composite image formation strategy in Ref. 1, which we summarize next. The idea is to use a bank of K matched filters, each characterized by a center response azimuth and a response width and shape.[4,5] Each of these matched filter outputs is an image conventionally reconstructed from a subaperture of the full azimuth aperture. The underlying assumption is that it is reasonable to assume isotropic scattering within the angular extent of these subapertures. Given the subaperture images $\hat{\mathbf{f}}^k$ for all subapertures $k \in \{1, ..., K\}$, the composite image $\hat{\mathbf{f}}$ is formed as follows:

$$\hat{\mathbf{f}}_{ij} = \arg\max_k \hat{\mathbf{f}}^k_{ij} \tag{1}$$

where $\hat{\mathbf{f}}^k_{ij}$ and $\hat{\mathbf{f}}_{ij}$ denote the (i,j)-th pixel of the k-th subaperture image and of the composite image, respectively. Thus, the composite image has the interpretation of a Generalized Likelihood Ratio Test (GLRT) statistic for scattering responses with known response shape[4,5] but with unknown peak response angle. We note that in addition to the reflectivity estimates, there is more information available at the output of this process, namely for each pixel we know the index k of the corresponding subaperture image at which the maximum occurs. This provides some characterization of the aspect dependence of the scatterers, which may be useful for aiding object visualization or for use in an automatic target recognition algorithm.

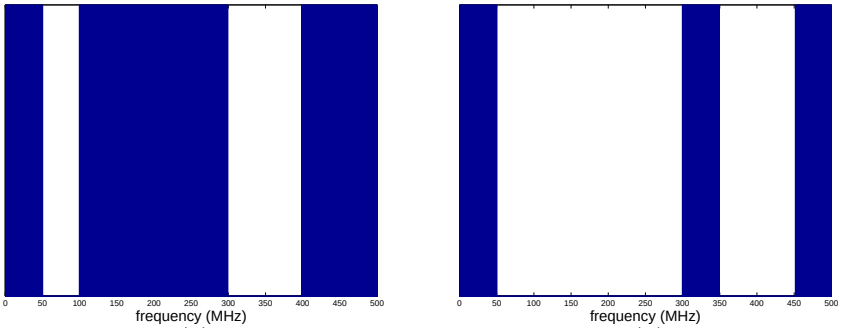

Figure 3. Two patterns of frequency-band omissions, dark regions indicating bands where data are available and light regions indicating missing bands. The masks in (a) and (b) lead to 70% and 30% of the data from the full band being available, respectively.

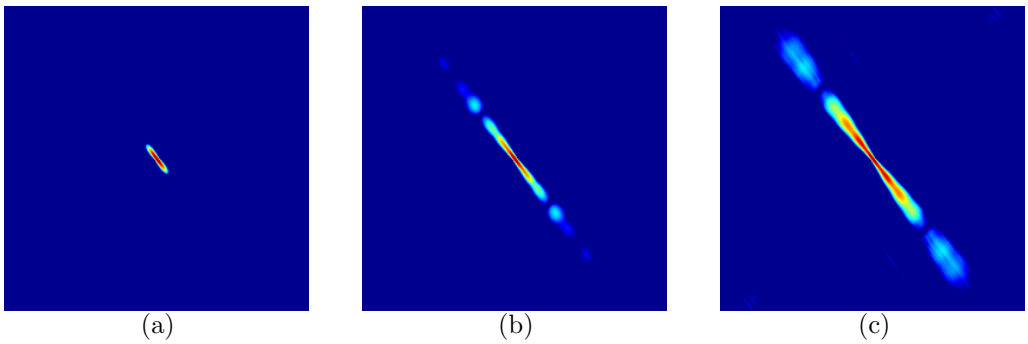

Figure 4. Conventionally reconstructed images of a point scatterer based on data from a 20° subaperture centered at 45°. The images show a region of 10×10 meters. (a) Full frequency band available. (b) 70% of the frequency band available. (c) 30% of the frequency band available.

For illustration, let us view the PSFs corresponding to a single subaperture image that would then be used in composite image formation. In particular, let us consider a subaperture of the data shown in Fig. 1, which is centered at 45° and which has a width of 20°. The PSF for the case of no frequency-band omissions is shown in Fig. 4(a), which is essentially a sinc-like response wider in the range direction than in the cross-range direction. The PSFs for the frequency-band omissions corresponding to the two patterns in Fig. 3 are shown in Fig. 4(b) and 4(c). We note that frequency-band omissions cause significant widening of the PSFs, implying that if conventionally formed subaperture images are used in composite image formation, the final image will suffer from significant artifacts. In the next section, we consider an alternative strategy to address this issue.

2.3. Model-based, Point-enhanced Composite Image Formation

For subaperture image formation, we consider an approach based on the feature-enhanced image formation framework of Ref. 2. In particular, in this paper we focus on resolving and enhancing spatially-localized features, and consider the point-enhanced imaging idea of Ref. 2. This imaging technique can use data in the phase history, the range profile, or the spatial domain. Here we consider the version where we use the conventional image as the input data, hence the technique works as a deconvolution method. In particular, let $\mathbf{y}^k$ be the conventionally reconstructed k-th subaperture image, and let $\mathbf{H}^k$ be a matrix each row of which contains a spatially shifted version of the corresponding PSF (stacked as a row vector). Then point-enhanced subaperture imaging is achieved by solving the following optimization problem:

$$\hat{\mathbf{f}}^k = \arg\min_{\mathbf{f}} \left\{ \|\mathbf{y}^k - \mathbf{H}^k\mathbf{f}\|_2^2 + \lambda\|\mathbf{f}\|_1 \right\} \tag{2}$$

where λ is a scalar parameter. The first term in the objective function of Eqn. (2) is a data fidelity term, incorporating the mathematical model of the observation process $\mathbf{H}^k$ into imaging. The second term enforces sparsity of the reconstructed image, which can lead to superresolution in the case of scenes containing a relatively small number of spatially-localized scatterers. The optimization problem in Eqn. (2) can be solved by using efficient iterative algorithms. We note that this expression is written in matrix-vector form for convenience, however in practice we avoid explicitly forming the large matrices $\mathbf{H}^k$ (hence we reduce the memory requirements), by noting that the matrix vector products can be carried out by convolutional operations. Given such point-enhanced subaperture images, we again form composite images as described in Section 2.2, with the only change of replacing the conventional subaperture images with the point-enhanced ones. Note that this procedure again produces more than just an image of reflectivities, since we also obtain a characterization of the aspect dependence of each scatterer.

3. EXPERIMENTAL RESULTS

We present 2D image reconstruction experiments based on the AFRL "Backhoe Data Dome, Version 1.0," which consists of simulated wideband (7-13 GHz), full polarization, complex backscatter data from a backhoe vehicle in free space.[3] The backscatter data are available over a full upper 2π steradian viewing hemisphere. In our experiments, we use VV polarization data, centered at 10 GHz, and with an azimuthal span of 110° (centered at 45°). We consider four different bandwidths: 500 MHz, 1 GHz, 2 GHz, and 4 GHz. For each of these four bandwidths, we consider both the case of full-bandwidth data, and the case of frequency-band omissions where 70% or 30% of the spectral data within that bandwidth are available. For frequency-band omissions, we use the two masks in Fig. 3 with appropriate scaling to the corresponding bandwidth. For composite imaging, we use 19 subapertures, with azimuth centers at 0°, 5°, ..., 90°, each with an azimuthal width of 20°. The response shape for each subaperture is chosen to be a Hamming window.

3.1. Linear Aperture

First we consider data that would correspond to a linear flight path of the radar platform. In particular, we use azimuth and elevation pairs that simulate such a linear aperture, with a peak elevation angle (at azimuth center) of 30°. In Fig. 5 we show images of the backhoe reconstructed from such data with various bandwidths. The composite images in Fig. 5(b) appear to provide larger response amplitudes for narrow-aperture scattering centers as compared to the conventional images in Fig. 5(a). This is because the conventional coherent integration process averages all scatterers (including those with a narrow-angle persistence) over the entire wide-angle azimuthal aperture. We note that these two types of images exhibit similar resolution properties and mainlobe structure for the scatterers. As bandwidth is reduced, some features of the backhoe appear to be lost in the images in Fig. 5(a) and 5(b). In contrast, the corresponding composite, point-enhanced images in Fig. 5(c) appear to preserve and exhibit some of the features present in higher-bandwidth images. We choose the hyperparameter λ in Eqn. (2) by visual assessment of the formed imagery. Automatic hyperparameter choice is a topic of our current research. Next we consider frequency-band omissions. Fig. 6 contains results for the case where 70% of the band is available. We observe that conventional and composite images suffer from sidelobe artifacts, especially in the low-bandwidth cases. On the other hand, composite, point-enhanced images in Fig. 6(c) do not suffer from significant degradations as compared to the full-band versions in Fig. 5(c), exhibiting robustness to frequency-band omissions. Finally, in Fig. 7 we present results for the case where we have only 30% of the frequency band available. All imaging methods exhibit noticeable artifacts in this case, although composite, point-enhanced imaging is still able to localize significant scatterers and features of the backhoe.

3.2. Fixed Elevation

We now consider a different aperture, involving a fixed elevation of 0°, and present the results of an experimental analysis analogous to the one in the previous section. The results shown in Figs. 8-10 lead to similar observations.

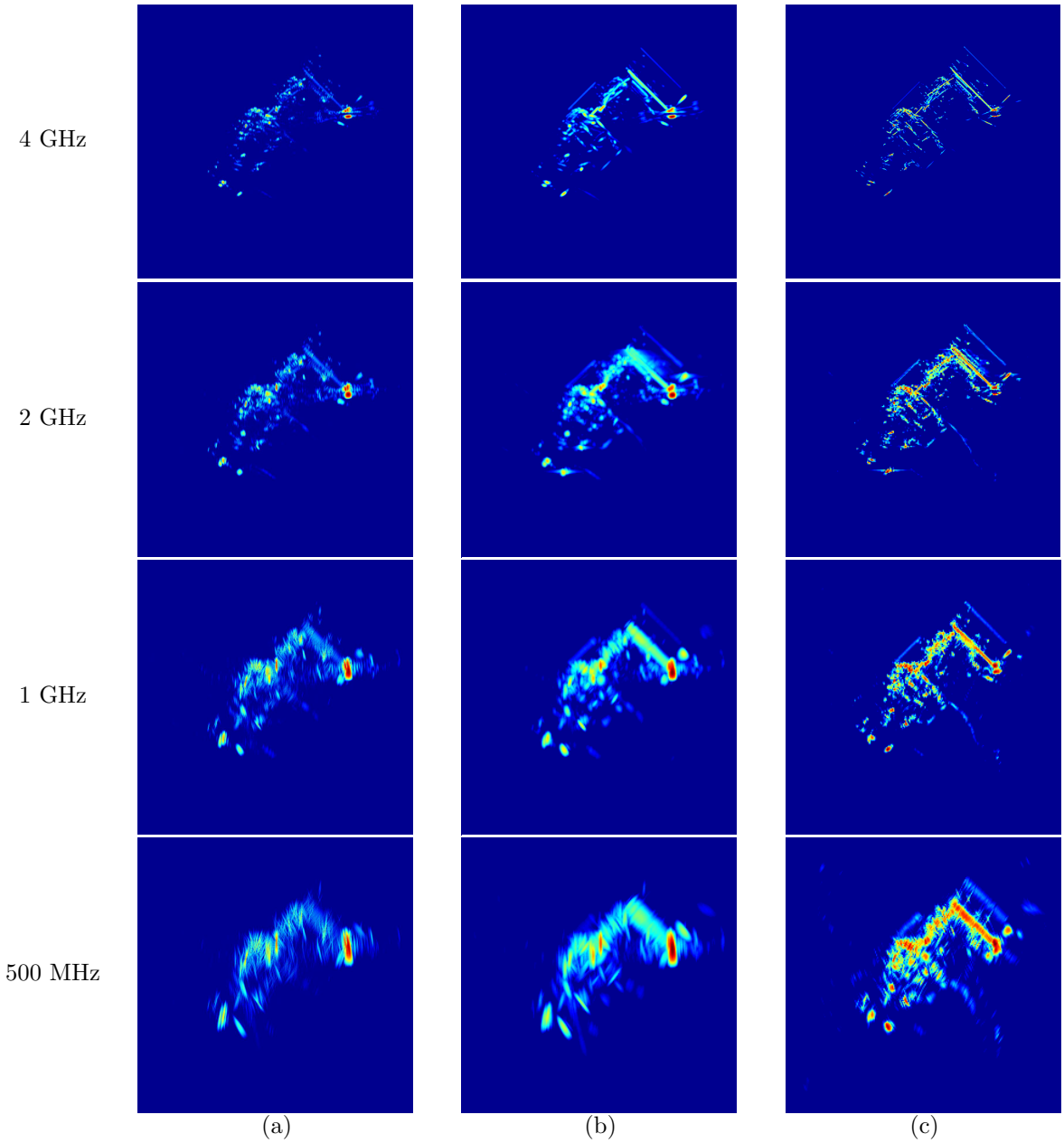

Figure 5. SAR images of the backhoe using a linear aperture and bandwidths of 4 GHz, 2 GHz, 1 GHz, and 500 MHz. (a) Conventional imaging. (b) Composite imaging. (c) Composite, point-enhanced imaging.

3.3. Visualization of Aspect Dependent Scattering

In the composite and composite, point-enhanced reconstruction results in the previous sections, we have only shown the reflectivities at each spatial location. However, as we pointed out in Section 2, we also have the knowledge of which subaperture has led to the maximum reflectivity for each spatial location. This in turn provides some information on the aspect dependence of each scatterer, namely the aspect providing the strongest return from that scatterer. Here we present one way of visualizing that information by encoding the maximum-response aspect through color. In particular, we color-code each pixel by one of 19 colors, corresponding to which of the 19 subapertures identified a maximum. We encode the peak amplitude in the brightness of the pixel. The

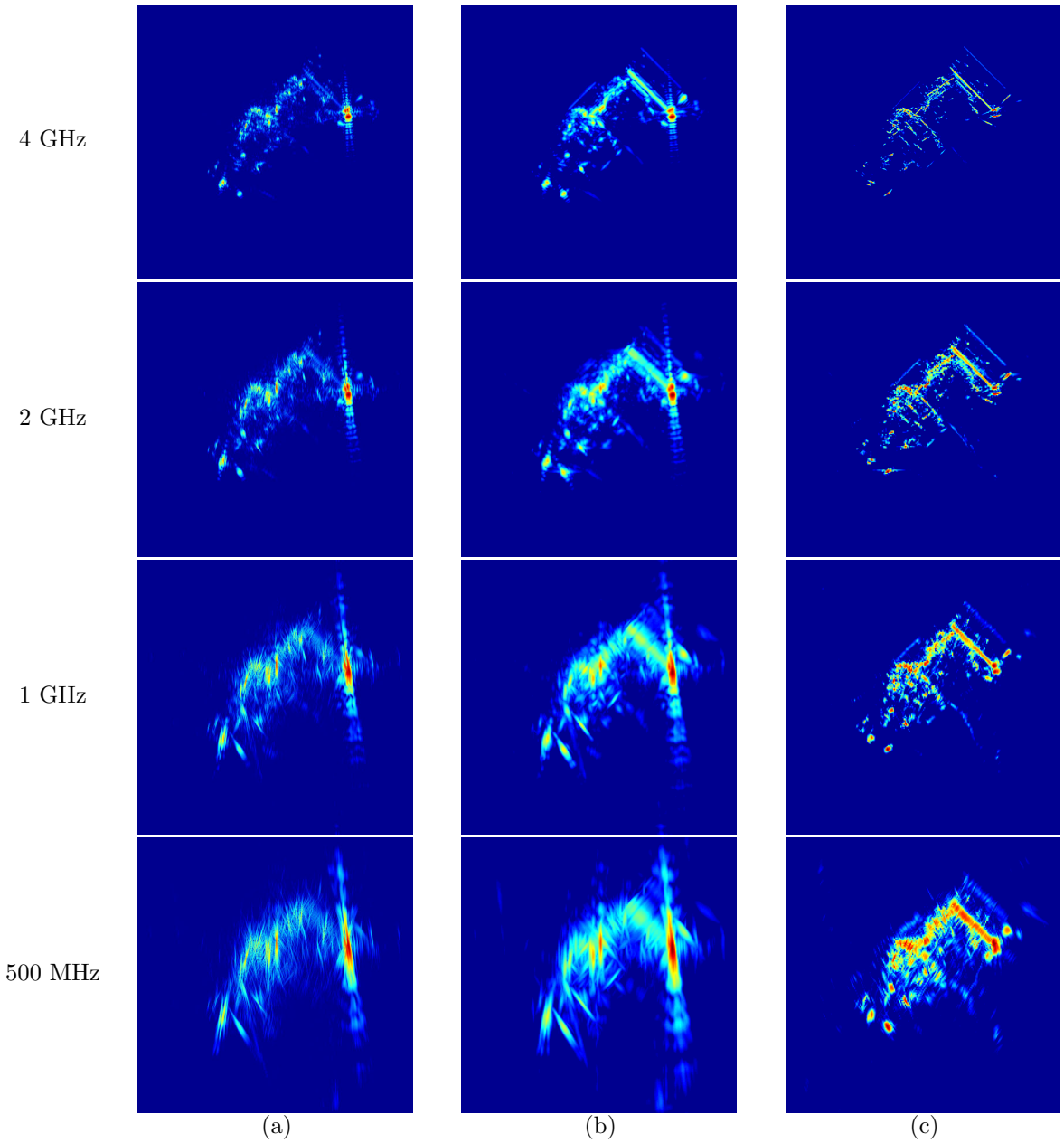

Figure 6. SAR images of the backhoe with frequency-band omissions (70% of the full-band data available) using a linear aperture and bandwidths of 4 GHz, 2 GHz, 1 GHz, and 500 MHz. (a) Conventional imaging. (b) Composite imaging. (c) Composite, point-enhanced imaging.

result is a color image, where red pixels denote maximum response at 0 degrees, green pixels at 45 degrees, and blue pixels at 90 degrees, with colors of intermediate hues representing the aspects in between, resulting in 19 colors each corresponding to a particular aspect. In Fig. 11, we show such color-coded versions of the composite and composite, point-enhanced reconstructions of Fig. 6. These images, especially the point-enhanced ones, suggest that the aspect dependence information extracted in this manner can be informative, and may potentially be useful for scene interpretation, e.g. for target classification.

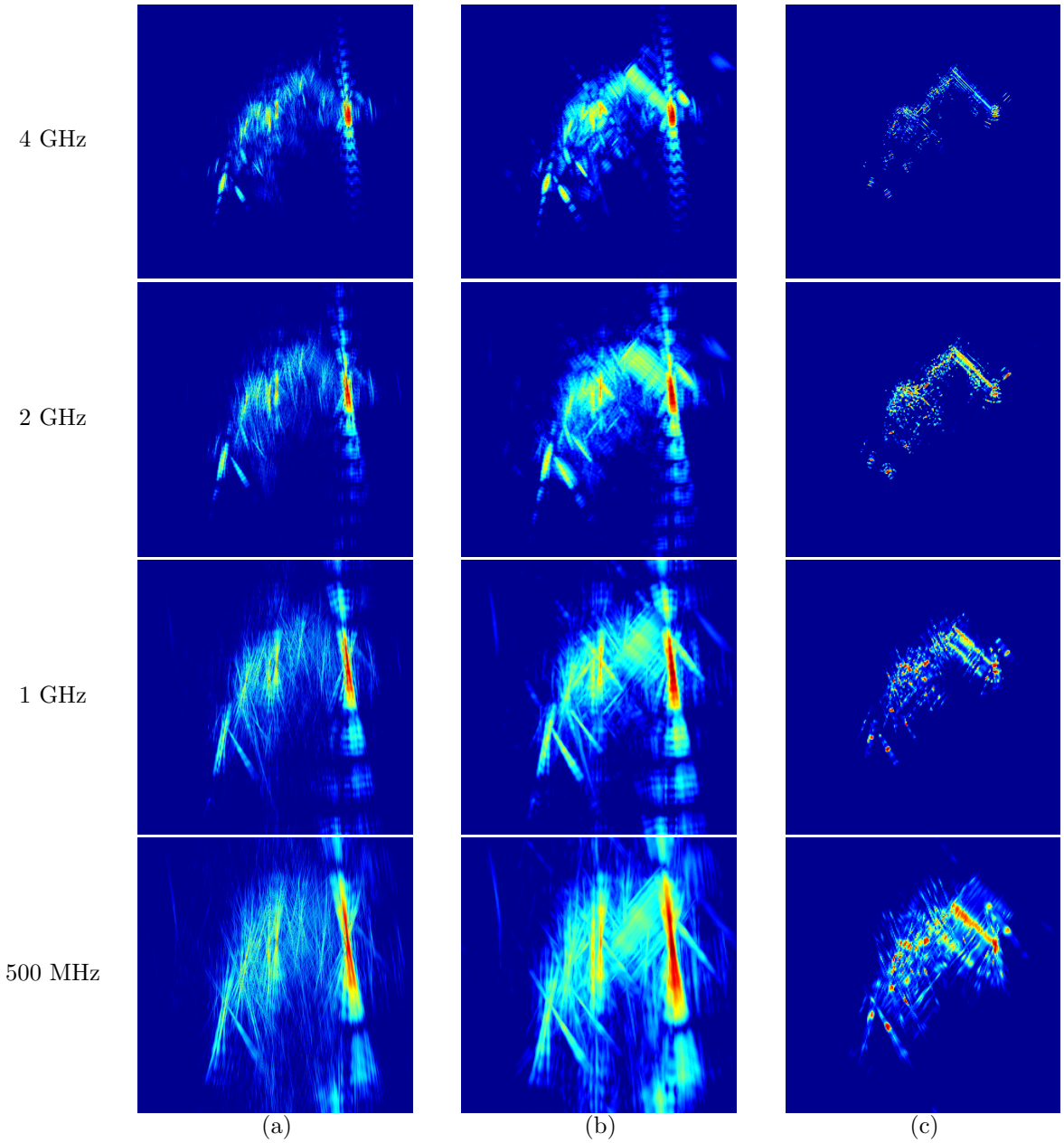

Figure 7. SAR images of the backhoe with frequency-band omissions (30% of the full-band data available) using a linear aperture and bandwidths of 4 GHz, 2 GHz, 1 GHz, and 500 MHz. (a) Conventional imaging. (b) Composite imaging. (c) Composite, point-enhanced imaging.

4. CONCLUSION

We have considered the problem of wide-angle SAR imaging from partial-aperture data with frequency-band omissions. We have proposed an approach that uses model-based, point-enhanced image reconstruction for narrow-angle subapertures, and then performs a nonlinear combination of the subaperture images to form a final wide-angle composite image. We have demonstrated that images formed in this manner exhibit robustness to bandwidth limitations as well as to frequency-band omissions. In addition, this approach yields a partial characterization of aspect dependence, which we have considered visualizing through a color-coding scheme.

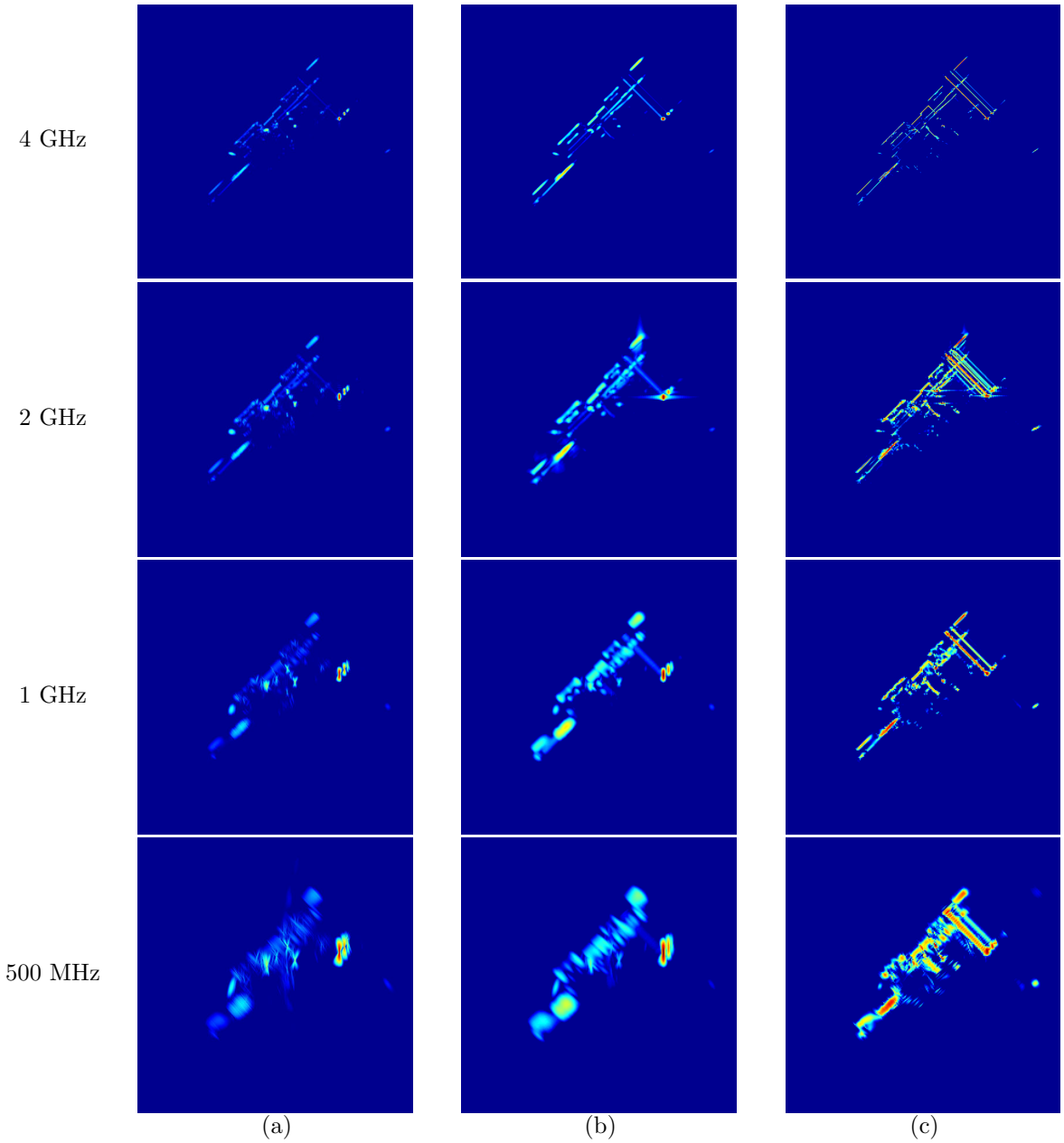

Figure 8. SAR images of the backhoe using a 0°-elevation aperture and bandwidths of 4 GHz, 2 GHz, 1 GHz, and 500 MHz. (a) Conventional imaging. (b) Composite imaging. (c) Composite, point-enhanced imaging.

Although we have considered only structured frequency-band omissions in this paper, the approach can also be applied to the case of unstructured omissions, as in random data dropouts. Similarly, these ideas can also be useful for the case of angle-band omissions. One important extension of this work could consider more precise characterization of angular anisotropy, by estimating the persistence level of each scatterer (which was assumed to be equal to the subaperture extent in this paper).

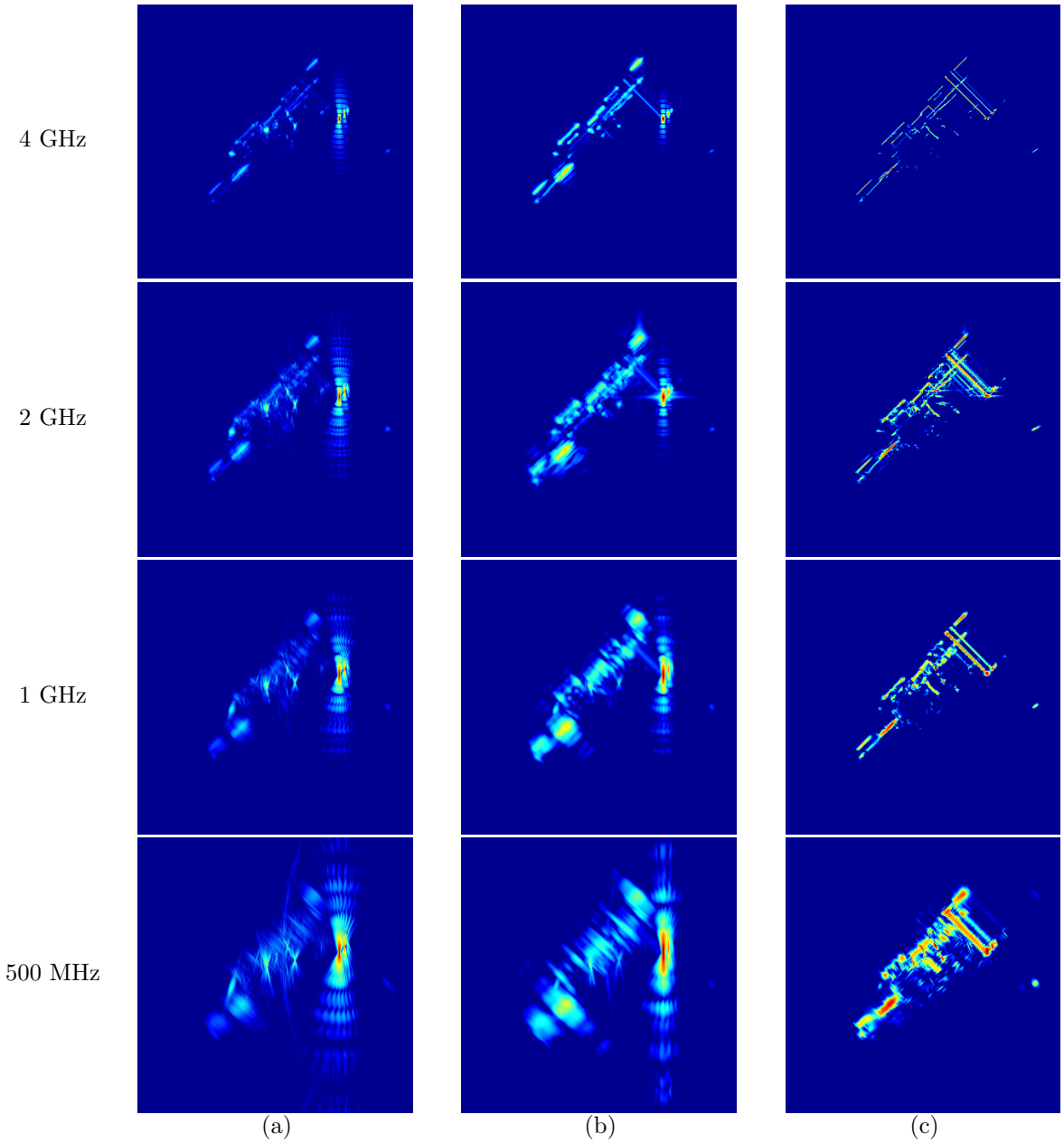

Figure 9. SAR images of the backhoe with frequency-band omissions (70% of the full-band data available) using a 0°-elevation aperture and bandwidths of 4 GHz, 2 GHz, 1 GHz, and 500 MHz. (a) Conventional imaging. (b) Composite imaging. (c) Composite, point-enhanced imaging.

ACKNOWLEDGMENTS

This work was supported by the Air Force Research Laboratory (AFRL) under Grant FA8650-04-1-1719, and by the Air Force Office of Scientific Research (AFOSR) under Grant F49620-00-0362.

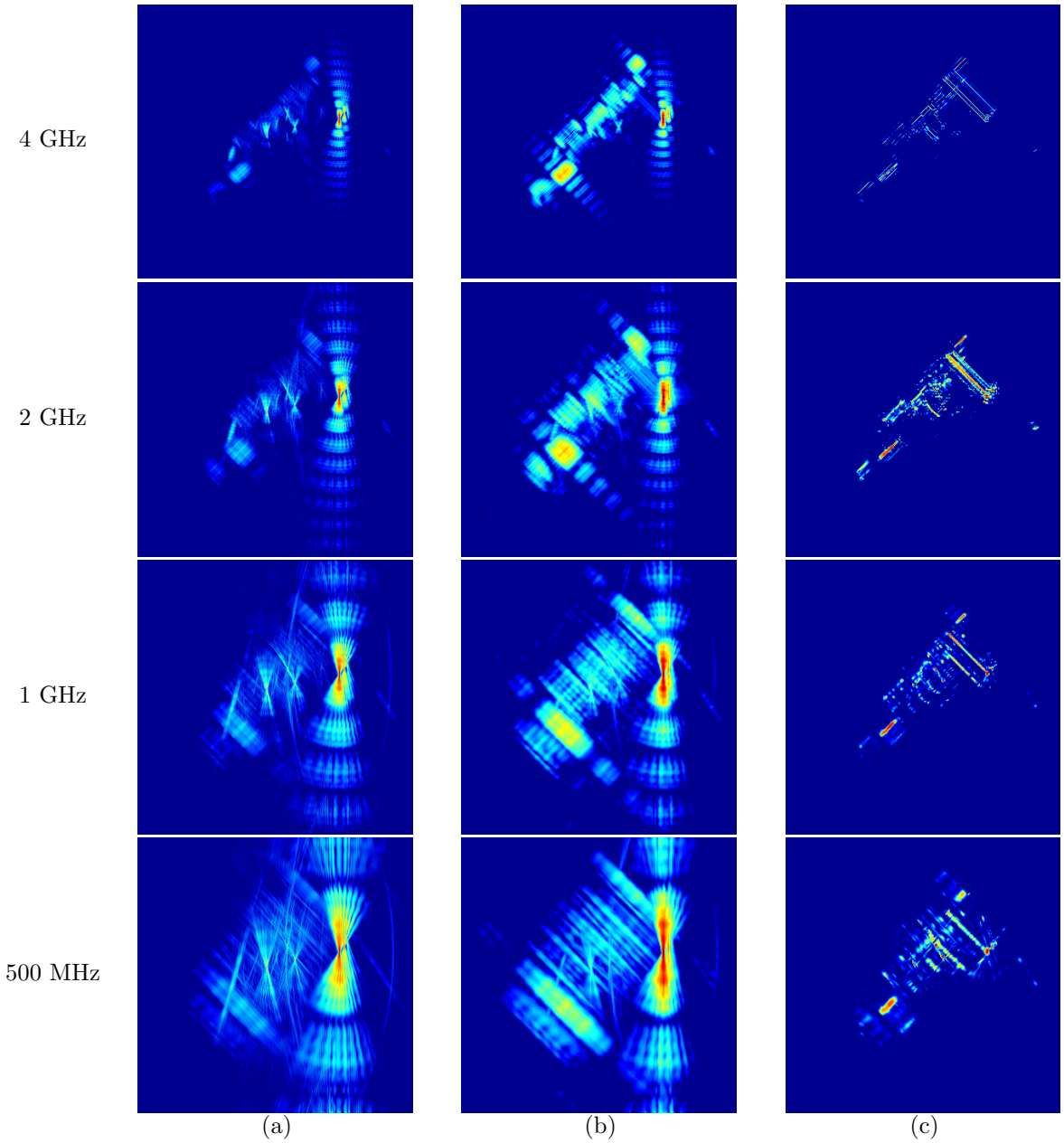

Figure 10. SAR images of the backhoe with frequency-band omissions (30% of the full-band data available) using a 0°-elevation aperture and bandwidths of 4 GHz, 2 GHz, 1 GHz, and 500 MHz. (a) Conventional imaging. (b) Composite imaging. (c) Composite, point-enhanced imaging.

REFERENCES

1. R. L. Moses, L. Potter, and M. Çetin, "Wide angle SAR imaging," in *Algorithms for Synthetic Aperture Radar Imagery XI*, E. G. Zelnio and F. D. Garber, eds., *Proc. SPIE*, (Orlando, FL, USA), Apr. 2004.
2. M. Çetin and W. C. Karl, "Feature-enhanced synthetic aperture radar image formation based on nonquadratic regularization," *IEEE Trans. Image Processing* **10**, pp. 623–631, Apr. 2001.
3. "Backhoe Data Sample & Visual-D Challenge Problem available through the Air Force Research Laboratory Sensor Data Management System Web Page: https://www.sdms.afrl.af.mil/main.htm."

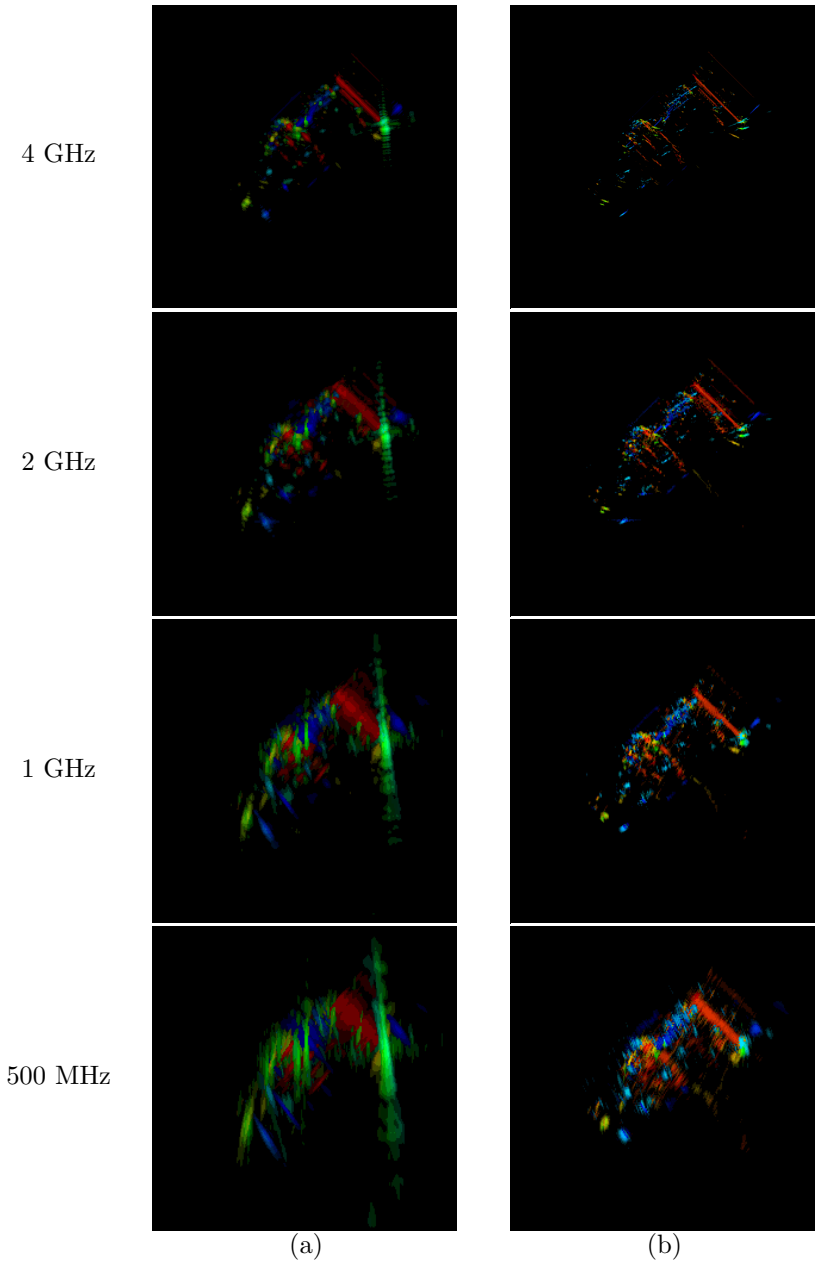

Figure 11. Visualization of aspect dependence. Angle-encoded SAR images of the backhoe with frequency-band omissions (70% of the full-band data available) using a linear aperture and bandwidths of 4 GHz, 2 GHz, 1 GHz, and 500 MHz. (a) Composite imaging. (b) Composite, point-enhanced imaging.

4. M. R. Allen and L. E. Hoff, "Wide-angle wideband SAR matched filter image formation for enhanced detection performance," in *Algorithms for Synthetic Aperture Radar Imagery*, **2230**, pp. 302–314, SPIE, (Orlando, FL, USA), Apr. 1994.
5. R. D. Chaney, A. S. Willsky, and L. M. Novak, "Coherent aspect-dependent SAR image formation," in *Algorithms for Synthetic Aperture Radar Imagery*, **2230**, pp. 256–274, SPIE, (Orlando, FL, USA), Apr. 1994.